SUPPORTING INFORMATION

Electrically controllable light-trapping for self-powered switchable solar windows

Joseph Murray[†,‡]*, Dakang Ma*[†,‡] *and Jeremy N. Munday*[†,‡]

[†]Department of Electrical and Computer Engineering, University of Maryland, College Park, 20742, USA

[‡]Institute for Research in Electronics and Applied Physics, University of Maryland, College Park, MD 20740, USA

Fitting Optical Parameters

The optical parameters were jointly fit using ellipsometry, AFM measurements, and integrating sphere measurements (absorption and transmission). Figure S1 shows the comparison between measured (open circles) and modeled (solid line) absorption, using joint fits for the four films used in this work. All fits have less than 1% root mean squared (RMS) error between measurement and modeling results. Similarly, Figure S2 shows measured (open circles) and modeled (solid line) absorption and transmission used in characterizing the PDLC layers (note that this is for the side of the device without the a-Si layer). The characterization methodology is described in Ref[1]. Figure S3 shows the AFM measurements used to determine film thickness

and roughness. The step heights were produced by partially covering samples during film deposition.

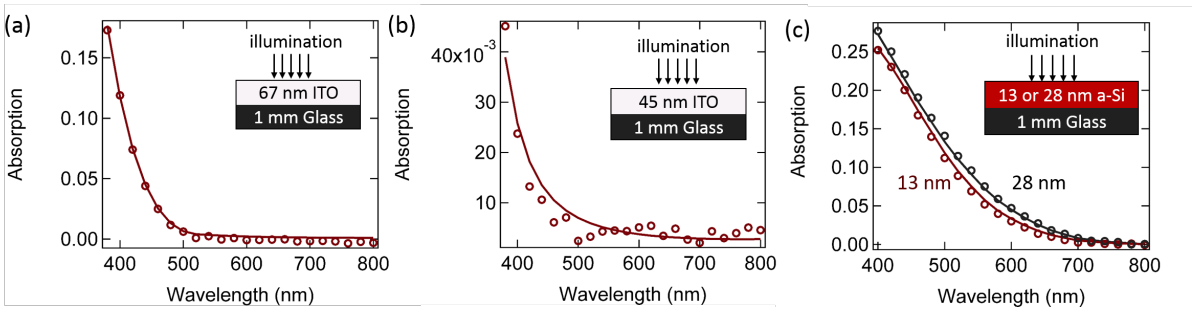

Figure S1. Thin-film absorption measurements and modeling. Measured (open circles) and calculated (solid lines) absorption for (a) the top ITO, (b) the bottom ITO, and (c) the a-Si layers (top and bottom refer to schematic in Figure 1). The modeled data are the result of a joint fit of ellipsometric data, AFM, and absorption data.

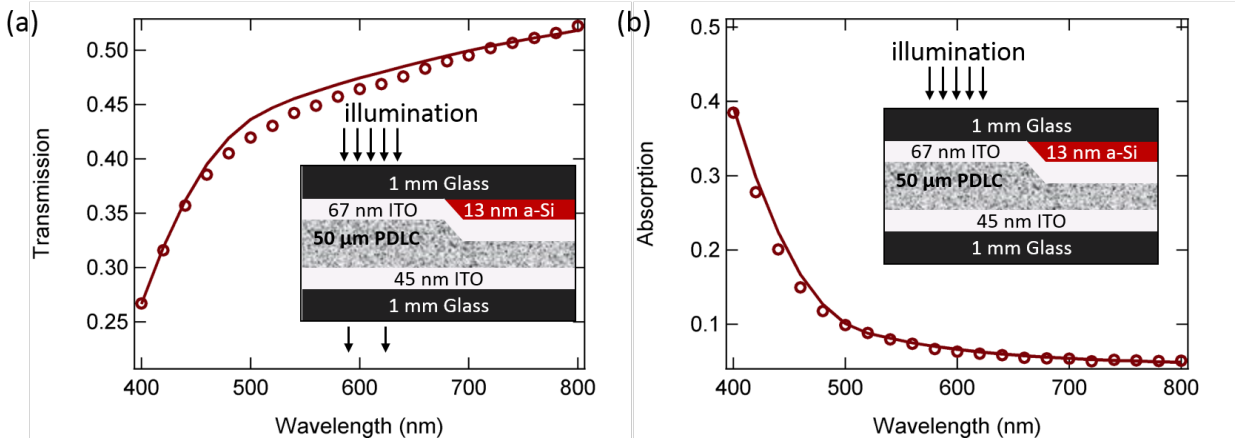

Figure S2. PDLC characterization. Measured (open circles) and the calculated (solid lines) absorption in the PDLC cell (side without a-Si). This measurement allows for fitting of the PDLC parameters that are necessary for accurate optical modeling of the scattering, as outlined in Ref[1].

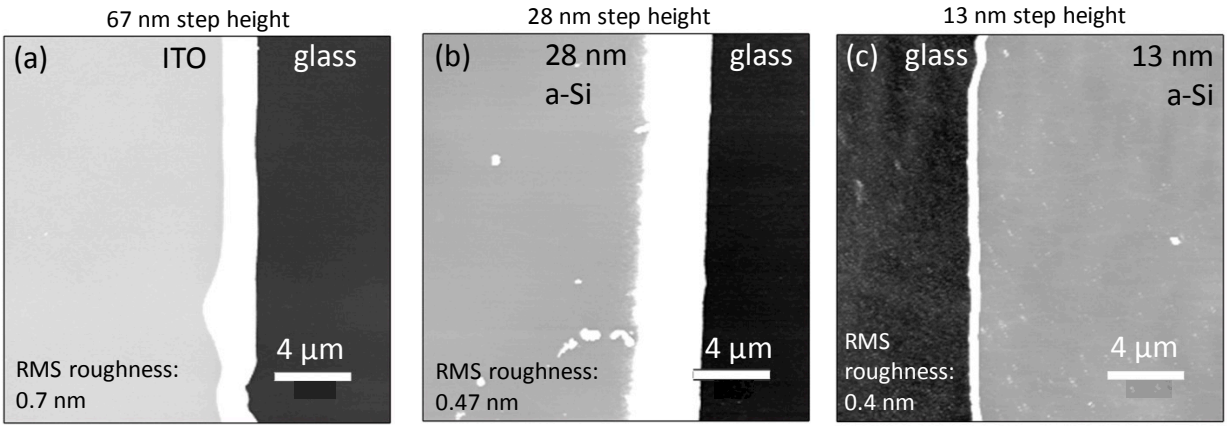

Figure S3. AFM step height measurements used to determine thickness of (a) the top ITO layer, (b) the 28 nm a-Si layer, and (c) the 13 nm a-Si. RMS surface roughnesses are 0.7 nm, 0.47 nm, and 0.4 nm, respectively. Step heights were produced by partially covering the samples during deposition. Bottom ITO was not manufactured in house and so no step height was available.

Calculating Absorption

Absorption and transmission in the ON state were calculated by Fresnel coefficients using the matrix transfer method including coherent reflection/transmission (for thin-films) and incoherent reflection/transmission (for thick layers such as the glass and PDLC layer) following Katsidis and Siapkas[2]. This method uses field transfer matrices to calculate the intensity of reflection/transmission between incoherent layers (or to outside the structure) and then intensity transfer matrices to calculate the total reflection/transmission. Total absorption and transmission in the OFF state were calculated using the effective index ensemble method[3] and the per layer absorption was calculated using the model developed in Ref[1].

Calculating power generation

Power generation was calculated using a single diode model with current density, $J(V)$, calculated as a function of voltage, V, by:

$$J(V) = J_o\left(1 - \exp\left({}^{V}/_{V_{th}}\right)\right) + J_{sc,calc}\ , \tag{1}$$

where V_{th} is the thermal voltage (25.9 mV at 300 K), J_o is the reverse saturation current density (see below), and $J_{sc,calc}$ is the predicted short circuit current density based on the calculated absorption, which is given by:

$$J_{sc,calc} = q\int_0^\infty S_{AM1.5G}(\lambda) * A_{calc}(\lambda) * \left({}^{\lambda}/_{hc}\right)d\lambda\ , \tag{2}$$

where λ is the wavelength, h is Planck's constant, q is the electron charge, c is the speed of light in vacuum, $S_{AM1.5G}(\lambda)$ is the spectral power density for Air Mass 1.5 Global illumination, and $A_{calc}(\lambda)$ is the calculated absorption in the a-Si layer using the methods described above. J_o is extrapolated from a high quality a-Si solar cell,[4] based on the measured open-circuit voltage, $V_{oc,cell}$, and the short-circuit current, $J_{sc,cell}$, using:

$$J_o = \frac{J_{sc,cell}}{\exp\left({}^{V_{oc,cell}}/_{V_{th}}\right)}\ . \tag{3}$$

The power generation, P, is:

$$P = \max(J(V) * V) \,. \tag{4}$$

Note that our goal here is to create a simple but reasonable model for the power generation of a state of the art cell incorporated into our device using experimentally determined values of the cell parameters (Figure S4).

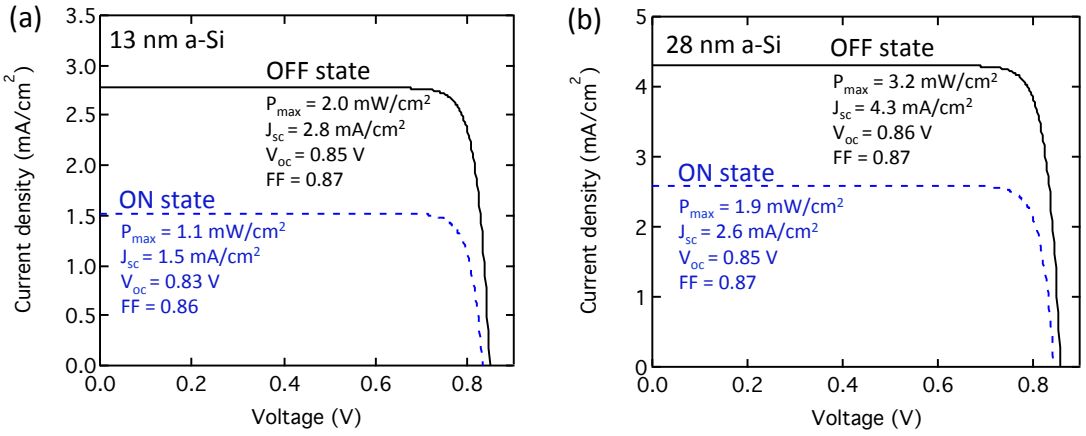

Figure S4. Modeled performance of solar cells comprised of (a) 13 nm and (b) 28 nm of a-Si. Current density as a function of voltage is shown and relevant parameters are given in the insets for both the ON and OFF states.

Characterizing scattering

We used a glass hemisphere and the technique described in Ref[3] to determine the internal scattering characteristics. The hemispherical technique allows for determination of all scattering from the PDLC layer. Figure S5 shows a schematic depiction of the technique. An important assumption of the absorption calculations is that light is fully randomized in the PDLC layer, and the validity of this assumption is demonstrated in Figure S5. This plot shows the normalized scattering angle versus reflected angle with overlapping traces for incident angles between 5° and 30° (at higher angles specular reflection becomes too strong be to completely removed with the crossed polarizers). If light were not fully randomized in the PDLC layer, the scattering

would depend on incident angle. However, no dependence is observed with relative RMS variations about the mean of only 3%.

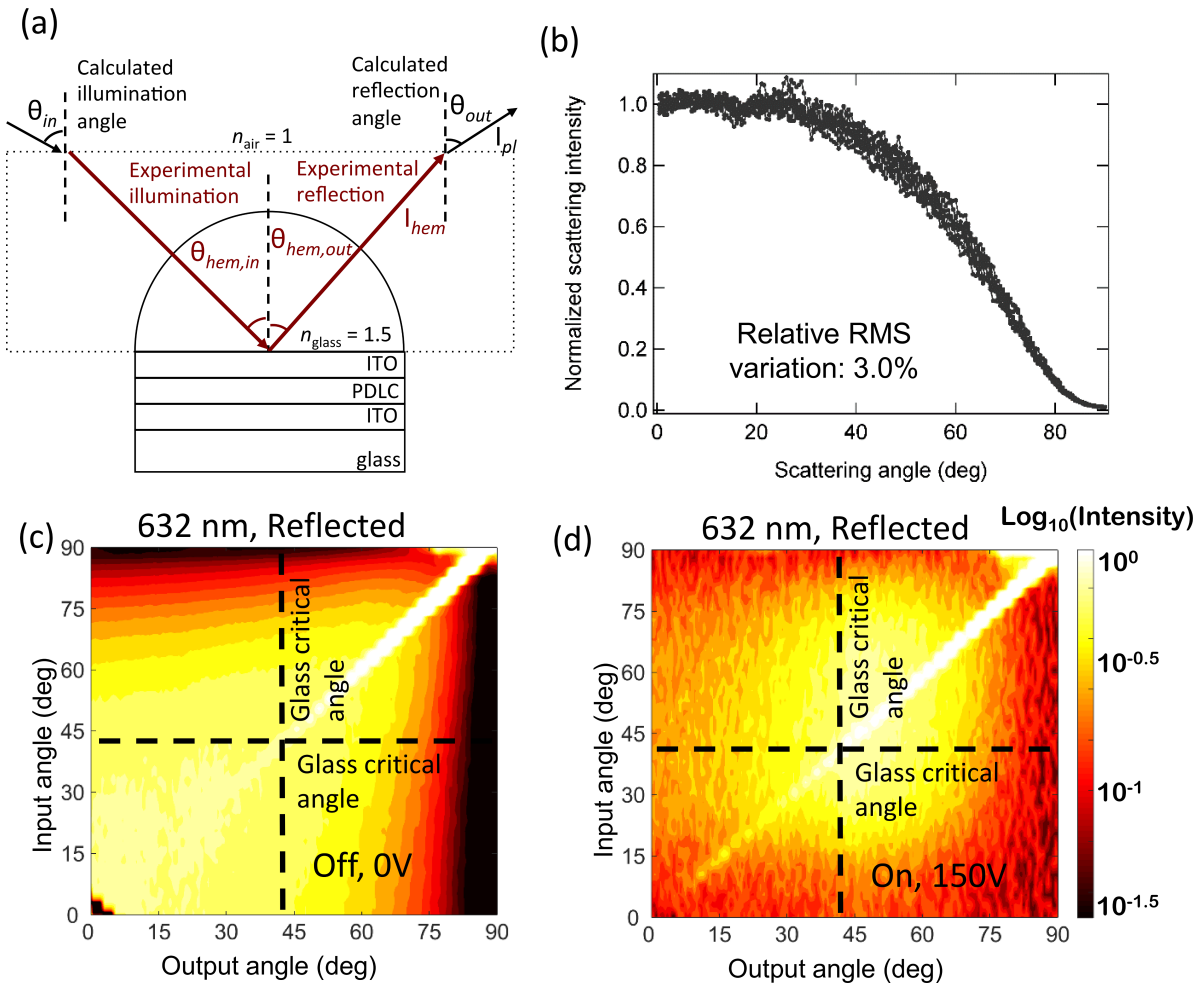

Figure S5. Determination of the scattering within a PDLC device. (a) A glass hemisphere allows for illumination and observation of all internal reflected scattering[3], for the purposes of modeling and extrapolating to other device configurations. Reflected scattered intensity as a function of input (illumination) angle and output (observation) angle with the device in the (c) OFF and (d) ON states. Note that only the bottom left corner of these graphs represent observable angles for a purely planar device (*i.e.* the hemisphere enables the determination of the scattering intensities in the other three quardants).

Figure S5c,d shows the reflected scattering intensity as a function of incident illumination for the (c) OFF and (d) ON states. The use of the BK7 hemisphere enables complete characterization of the optical scattering within the device; however, only the data from the lower left quadrant is

used to obtain the data in the inset of Figure 5 of the main text. The scattering angles ($\theta_{hem,out}$) and illumination angles ($\theta_{hem,in}$) shown in Figure S5, were mapped to the scattering and illumination angles (θ_{out} and θ_{in} , respectively) shown in the inset of Figure 5 for a planar device by Snell's law, using the glass index of 1.5:

$$\theta_{out} = \sin^{-1}\big(1.5\sin(\theta_{hem,out})\big) \tag{5a}$$

and

$$\theta_{in} = \sin^{-1}\big(1.5\sin(\theta_{hem,in})\big). \tag{5b}$$

The scattering intensity is also transformed to account for the differing geometry between the hemisphere and the planar slab. First, the change in intensity due to the above change in propagation angle is accounted for by multiplying by the ratio of cosines ($\cos(\theta_{out})/\cos(\theta_{hem,out})$) due to the increase in the solid angle for light exiting the planar slab. Second, with the hemisphere, all illumination and scattering angles experience the same transmission at the air/glass interface (*i.e.* the light is always normal to the surface), but the planar surface results in angle dependent transmission. Considering both effects, we have that the resulting intensity exiting the planar surface is:

$$I_{pl}(\theta_{in},\theta_{out}) = T(\theta_{in})T(\theta_{out})\frac{\cos(\theta_{out})}{\cos\big(\theta_{hem,out}\big)}I_{hem}\big(\theta_{hem,in},\theta_{hem,out}\big) \tag{6a}$$

$$= T(\theta_{in})T(\theta_{out})\frac{\cos(\theta_{out})\,I_{hem}\big(\theta_{hem,in},\theta_{hem,out}\big)}{\sqrt{1-\left(\frac{\sin(\theta_{out})}{1.5}\right)^2}} \tag{6b}$$

where T is the transmission coefficient, I_{pl} is the calculated scattering intensity for the planar geometry (shown in Figure 5), and I_{hem} is the measured intensity for the hemisphere (shown in Figure S5).

Transparency color perception

There is an important tradeoff between color perception and device performance in these experiments, as higher absorption and power generation can be achieved with thicker a-Si layers at the cost of lower transmission and greater tinting. To assess the color trade-off we calculate the chromaticity coordinates xyY based on the 1931 CIE system for color specification that gives the perceived color and perceived intensity for the human eye under a specified illumination. The illumination spectrum in this work is taken to be AM1.5G. The color matching functions $\bar{x}(\lambda)$, $\bar{y}(\lambda)$, and $\bar{z}(\lambda)$ describe the relative perception of red, green, and blue, color for a standard observer. For transmission $T(\lambda)$, the xyY coordinates are obtained as follows[5,6]:

$$k = \int_0^\infty S_{AM1.5G}(\lambda)\,\bar{y}(\lambda)d\lambda \tag{7a}$$

$$X = \frac{\int_0^\infty S_{AM1.5G}(\lambda)\,\bar{x}(\lambda)T(\lambda)d\lambda}{k} \tag{7b}$$

$$Y = \frac{\int_0^\infty S_{AM1.5G}(\lambda)\,\bar{y}(\lambda)T(\lambda)d\lambda}{k} \tag{7c}$$

$$Z = \frac{\int_0^\infty S_{AM1.5G}(\lambda)\,\bar{z}(\lambda)T(\lambda)d\lambda}{k} \tag{7d}$$

$$x = \frac{X}{X+Y+Z} \tag{7e}$$

$$y = \frac{Y}{X+Y+Z} \tag{7f}$$

$$z = \frac{Z}{X+Y+Z} \tag{7g}$$

where k is a normalizing constant, and X, Y, and Z are the tristimulus values. Because $x + y + z = 1$ only two of these values are needed to fully characterize the color. Figure S6 shows the xyY coordinates for the three a-Si samples shown in the main text for both the ON and

OFF states. This figure demonstrates the nearly colorless nature of the PDLC cell alone (0 nm a-Si). Increasing absorber thickness results in greater tinting and lower transmission.

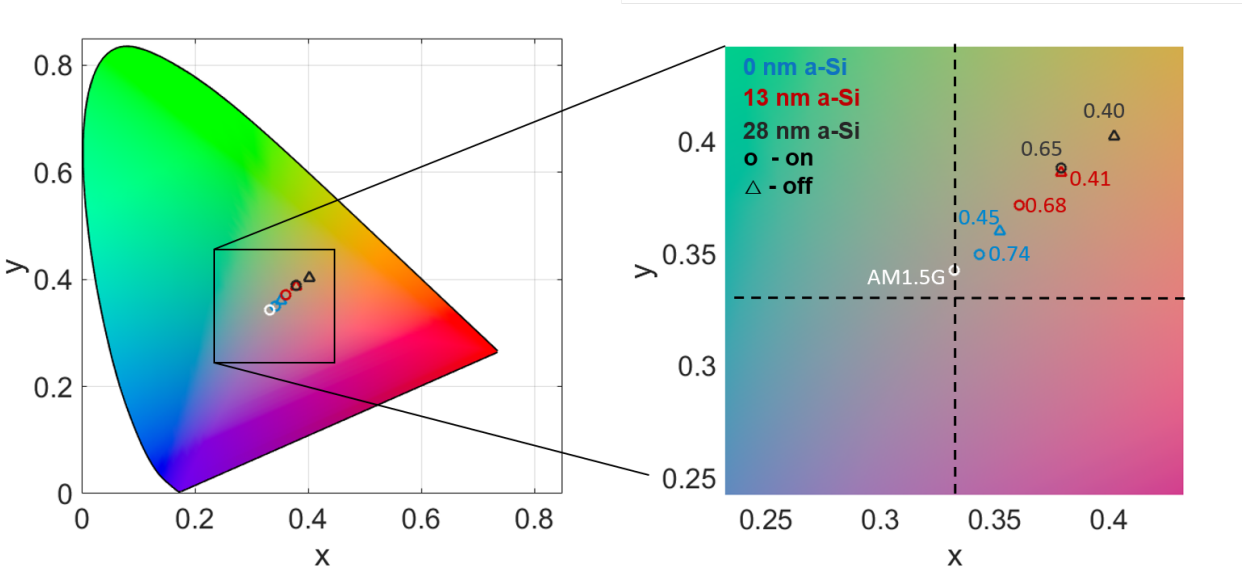

Figure S6. Chromaticity coordinates for the transmission of the devices investigated in this work overlaid on the CIE 1931 chromaticity diagram. The panel to the right shows an expanded view of the one on the left. In this expanded view the xy points are marked with their corresponding Y values.

(1) Murray, J. & Munday, J. N. A generalized approach to modeling absorption and photocurrent in solar cells with light scattering structures. J. Appl. Phys. 120, 165304 (2016).

(2) Katsidis, C. C.; Siapkas, D. I. General Transfer-Matrix Method for Optical Multilayer Systems with Coherent, Partially Coherent, and Incoherent Interference. *Appl. Opt.* **2002**, *41* (19), 3978–3987.

(3) Murray, J.; Munday, J. N. Experimental Demonstration and Modeling of the Internal Light Scattering Profile within Solar Cells due to Random Dielectric Scatterers. *J. Appl. Phys.* **2016**, *119* (2), 23104.

(4) Green, M. A.; Emery, K.; Hishikawa, Y.; Warta, W.; Dunlop, E. D. Solar Cell Efficiency Tables (Version 45). *Prog. Photovolt. Res. Appl.* **2015**, *23* (1), 1–9.

(5) Shevell, S. K. *The Science of Color*; Elsevier, 2003.

(6) Ameri, T.; Dennler, G.; Waldauf, C.; Azimi, H.; Seemann, A.; Forberich, K.; Hauch, J.; Scharber, M.; Hingerl, K.; Brabec, C. J. Fabrication, Optical Modeling, and Color Characterization of Semitransparent Bulk-Heterojunction Organic Solar Cells in an Inverted Structure. *Adv. Funct. Mater.* **2010**, *20* (10), 1592–1598.